

Experimental test of an extension of the Rosenzweig-Porter model to mixed integrable-chaotic systems experiencing time-reversal invariance violation

Xiaodong Zhang(张晓东), Jiongning Che(车炯宁), and Barbara Dietz

Citation: Chin. Phys. B, 2024, 33 (**12**): 120501. DOI: 10.1088/1674-1056/ad8a4e
Journal homepage: http://cpb.iphy.ac.cn; http://iopscience.iop.org/cpb

What follows is a list of articles you may be interested in

Resonance and antiresonance characteristics in linearly delayed Maryland model

Hsinchen Yu(于心澄), Dong Bai(柏栋), Peishan He(何佩珊), Xiaoping Zhang(张小平), Zhongzhou Ren(任中洲), and Qiang Zheng(郑强)
Chin. Phys. B, 2022, 31 (**12**): 120502. DOI: 10.1088/1674-1056/ac7a0d

Experimental investigation of the fluctuations in nonchaotic scattering in microwave billiards

Runzu Zhang(张润祖), Weihua Zhang(张为华), Barbara Dietz, Guozhi Chai(柴国志), Liang Huang(黄亮)
Chin. Phys. B, 2019, 28 (**10**): 100502. DOI: 10.1088/1674-1056/ab3f96

Dynamical stable-jump-stable-jump picture in a non-periodically driven quantum relativistic kicked rotor system

Hsincheng Yu(于心澄), Zhongzhou Ren(任中洲), Xin Zhang(张欣)
Chin. Phys. B, 2019, 28 (**2**): 020504. DOI: 10.1088/1674-1056/28/2/020504

Identifying the closeness of eigenstates in quantum many-body systems

Hai-bin Li(李海彬), Yang Yang(杨扬), Pei Wang(王沛), Xiao-guang Wang(王晓光)
Chin. Phys. B, 2017, 26 (**8**): 080502. DOI: 10.1088/1674-1056/26/8/080502

Level spacing statistics for two-dimensional massless Dirac billiards

Huang Liang (黄亮), Xu Hong-Ya (徐洪亚), Lai Ying-Cheng (来颖诚), Celso Grebogi
Chin. Phys. B, 2014, 23 (**7**): 070507. DOI: 10.1088/1674-1056/23/7/070507

Experimental test of an extension of the Rosenzweig–Porter model to mixed integrable-chaotic systems experiencing time-reversal invariance violation

Xiaodong Zhang(张晓东)[1,2], Jiongning Che(车炯宁)[3,1], and Barbara Dietz[2,4,1,†]

[1] *Lanzhou Center for Theoretical Physics, Key Laboratory of Theoretical Physics of Gansu Province, and Key Laboratory of Quantum Theory and Applications of the Ministry of Education, Lanzhou University, Lanzhou* 730000, *China*

[2] *Center for Theoretical Physics of Complex Systems, Institute for Basic Science (IBS), Daejeon* 34126, *Korea*

[3] *Yangtze Delta Region Institute, University of Electronic Science and Technology of China, Huzhou* 313001, *China*

[4] *Basic Science Program, Korea University of Science and Technology (UST), Daejeon* 34113, *Korea*

(Received 14 September 2024; revised manuscript received 14 October 2024; accepted manuscript online 23 October 2024)

We report on the theoretical and experimental investigations of the transition of a typical quantum system with mixed regular-integrable classical dynamics to one with violated time-reversal ($\mathcal{T}$) invariance. The measurements are performed with a flat superconducting microwave resonator with circular shape in which chaoticity is induced by using either long antennas or inserting two circular disks into the cavity, and by magnetizing a ferrite disk placed at its center, which leads to violation of $\mathcal{T}$ invariance. We propose an extension of the Rosenzweig–Porter (RP) model, which interpolates between mixed regular-chaotic instead of integrable dynamics and fully chaotic dynamics with violated $\mathcal{T}$-invariance, and derive a Wigner-surmise like analytical expression for the corresponding nearest-neighbor spacing distribution. We propose a procedure involving this result and those for the RP model to determine the size of $\mathcal{T}$-invariance violation and chaoticity and validate it employing the experimental eigenfrequency spectra.

Keywords: wave chaos, quantum chaos, quantum billiards, microwave billiards, random matrix theory, microwave experiments

PACS: 05.45.Mt, 03.65.Sq, 41.20.Jb, 05.45.Gg **DOI:** 10.1088/1674-1056/ad8a4e

1. Introduction

The objective of quantum chaos[1–3] is to identify signatures of classical chaos in the fluctuation properties of the eigenvalue spectrum and the features of the wave functions of the corresponding quantum system. Concerning the spectral properties of typical quantum systems two conjectures have been formulated. According to the Berry–Tabor conjecture,[4] the eigenvalues of quantum systems with an integrable classical counterpart exhibit Poissonian statistics classified with $\beta = 0$. On the other hand, the Bohigas–Giannoni–Schmit conjecture[5–7] states that the spectral properties of typical quantum systems, whose corresponding classical dynamics is fully chaotic, are described by the Wigner–Dyson (WD) ensembles of random matrix theory (RMT). If time-reversal ($\mathcal{T}$) invariance is preserved, they are predicted to agree with those of random matrices from the Gaussian orthogonal ensemble (GOE) with $\beta = 1$, if it is violated with those of random matrices from the Gaussian unitary ensemble (GUE) with $\beta = 2$.[3,8] Indeed, in the past four decades RMT was successfully applied to analyze aspects of single-particle and many-body quantum chaos.[1–3,9–19] Originally, it was introduced by Wigner, who was the first to propose that there is a connection between their spectral properties and those of random matrices,[20–22] to describe properties of the eigenstates of complex many-body quantum systems like nuclei.[9,10,12,14,18,23] A paradigm model for the verification of the conjectures and the study of aspects of quantum chaos are quantum billiards (QBs) whose classical counterpart are two-dimensional billiards (CBs).[24–28] These consist of a bounded two-dimensional, simply-connected domain, in which a point-like particle moves freely and is reflected specularly at the boundary, and their dynamics depends only on the shape of the billiard. Numerous theoretical[1,3] and also experimental studies have been performed in the context of quantum chaos with microwave billiards (MBs) modeling QBs[29–35] and with microwave graphs modeling quantum graphs.[36–46]

Also, for typical systems with mixed regular-chaotic dynamics RMT models have been developed that interpolate between Poisson and WD statistics, for example the RP model[47–51] and the β ensembles for general β.[52,53] In Ref. [54] we investigated experimentally with a circular MB the properties of typical quantum systems undergoing a transition from Poisson to GUE statistics and validated analytical results for the corresponding RP model. An MB is a flat, cylindrical microwave resonator,[30,32,34,55] which is operated with microwaves whose frequencies are below the cut-off frequency $f^{\rm cut}$ of the first transverse-electric mode. In that frequency range the associated Helmholtz equation is scalar

†Corresponding author. E-mail: bdietzp@gmail.com

© 2024 Chinese Physical Society and IOP Publishing Ltd

and mathematically identical to the Schrödinger equation of the QB of the corresponding shape with Dirichlet boundary conditions (BCs). For typical $\mathcal{T}$-invariant systems with chaotic classical counterpart complete sequences of several 1000 eigenfrequencies[35,56,57] were obtained at liquid-helium temperature $T_{\rm LHe} = 4$ K with niobium and lead-coated microwave resonators that become superconducting at $T_{\rm c} = 9.2$ K and $T_{\rm c} = 7.2$ K, respectively. Quantum systems with chaotic classical dynamics and partially violated $\mathcal{T}$ invariance[58–62] were investigated experimentally in Refs. [63–65] and at room temperature in MBs.[33,36,39,40,66–70] In these experiments, $\mathcal{T}$ invariance was violated by inserting a ferrite into the MB and magnetizing it with an external magnetic field B. This is not possible at superconducting conditions with a lead-coated cavity[35] due to the Meissner–Ochsenfeld effect,[71] because lead is a superconductor of type I.[72] Accordingly, the top and bottom plates of the cavities used in Refs. [54,73] were made from niobium, which is a type-II[74] superconductor for 153 mT $\leq B \leq$ 268 mT, to realize MBs whose spectral properties undergo a transition from GOE to GUE, and from Poisson to GUE, respectively. The crucial advantage of superconducting MBs is, that complete sequences of about 1000 eigenfrequencies could be identified in these experiments, which would not be achievable with normal conducting MBs.

In this paper we present analytical and experimental results for the spectral properties of quantum systems with mixed regular-chaotic dynamics and preserved $\mathcal{T}$ invariance, that are subject to $\mathcal{T}$-invariance violation. The measurements were performed with superconducting MBs employing the same procedure as in Ref. [73] to induce $\mathcal{T}$-invariance violation. The basic MB has the shape of a ring billiard as in Ref. [54], and the transition from integrable to chaotic dynamics is realized by either using long antennas or inserting two circular disks, respectively. The objective is to develop a procedure for the determination of the size of chaoticity and of $\mathcal{T}$-invariance violation. For this we employ an extension of the RP model,[47] which is applicable to typical quantum systems experiencing a transition from Poisson to WD statistics, to one which is applicable when $\mathcal{T}$-invariance violation is induced in a quantum system with mixed regular-chaotic classical dynamics. The RP model was intensively studied about 3–4 decades ago,[60,62,75–82] and recently in the context of many-body quantum chaos and localization.[83–95]

2. Experiment

The experiments are performed at superconducting conditions with a circular MB with radius $R = 250$ mm which contains a ferrite disk with radius $R_0 = 30$ mm at its center. Photographs of the lid and basins of the MBs that were considered in this paper are shown in Fig. 1. As demonstrated in Ref. [54] the MB with just a ferrite at the center, referred to as MB1 in the following, emulates the spectral properties and length spectra of the corresponding ring QB, as illustrated in Fig. A1 in the Appendix A, implying that its classical dynamics is integrable. The cavity is constructed from three 5-mm thick plates, namely top and bottom niobium plates and a brass plate in between, which has a circular hole of radius $R = 250$ mm. The sidewall of the hole is coated with lead, and grooves were milled into the top and bottom surface of the middle plate along it. Furthermore, holes were milled out of all plates along circles; see Fig. 1. To realize a superconducting cavity with a high quality factor of $Q \gtrsim 5 \times 10^4$, the plates were screwed together tightly through these holes, tin-lead was filled into the grooves to attain a good electrical contact and the cavity was cooled down to below ≈ 5 K in a cryogenic chamber constructed by ULVAC Cryogenics in Kyoto, Japan. The cavity height, $h = 5$ mm, corresponds to a cutoff frequency $f^{\rm cut} = 30$ GHz.

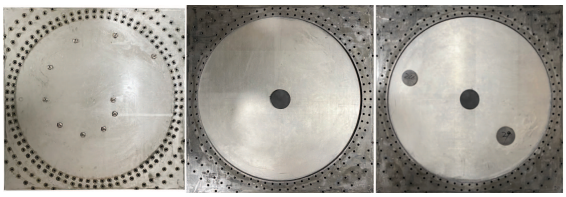


Fig. 1. Photograph of the niobium lid (left) and the basin of the MB which is formed by a 5-mm thick lead-coated brass plate with a circular hole of radius $R = 250$ mm on top of a niobium plate. The cavity MB1 contains a ferrite disk of radius $R_0 = 30$ mm at its center, mimicking a ring QB (middle) and additional lead-coated metallic disks for the cavity MB2 (right) in the experiments modelig a QB with mixed regular-chaotic dynamics.

The height of the ferrite disk equals h, corresponding to a cutoff frequency $f_{\rm F}^{\rm cut} \approx 4.5$ GHz and it is made of 19G3, whose saturation magnetization is $M_{\rm s} = 195$ mT and niobium is a superconductor of type II[74] as long as the magnetic field is chosen between two critical values, $B_{\rm c1} = 153$ mT and $B_{\rm c2} = 268$ mT. Namely, below $B_{\rm c1}$ it behaves like a superconductor of type I and above $B_{\rm c2}$ it becomes normal conducting.[96] Thus the ferrite could be magnetized at superconducting conditions with a static magnetic field of strength $B = 200$ mT generated by two external NdFeB magnets, thereby achieving partial $\mathcal{T}$-invariance violation at $T_{\rm LHe}$ and chaoticity.[54] We demonstrated in Ref. [97] that the spectral properties of a circular cavity which is loaded with a magnetized ferrite material, agree above the cut-off frequency with those of a classically chaotic quantum system with a mirror symmetry and completely violated $\mathcal{T}$ invariance. Thus, the magnetized ferrite disk acts like a random potential.[54]

In total 10 antenna ports were fixed to the lid. In the experiments emulating a ring QB, the lengths of the antennas were chosen such that they reached 0.5 mm into the cavity, to ensure that all resonances are excited, that the cavity has a high quality factor and that it is optimally closed. Note, that one long antenna suffices to change the spectral properties of an MB with the shape of a typical integrable

CB from Poissonian to intermediate statistics. The long antenna is accounted for in the associated Helmholtz equation by a delta-function potential with a frequency-dependent amplitude, implying that the strength of the perturbation caused by it increases with frequency.[98] Actually, it has been demonstrated in Refs. [98–101] that such MBs emulate singular billiards.[102–107] Thus, to attain an MB modelig a QB whose classical dynamics is not singular, but integrable with a small chaotic part, we used 10 long antennas, that reached 2 mm into the cavity. To realize an MB, denoted as MB2 in the following, which simulates a QB with mixed regular-chaotic classical dynamics with a large chaotic part, we inserted two lead-coated copper disks with radii 24 mm and 29 mm into the MB1. Note, that in Ref. [108] we performed experiments with a large-scale circle-sector shaped MB which contained metallic disks, whose sizes were sufficiently small as compared to that of the MB, to model QBs with nearly-integrable classical dynamics, whereas in the present experiments the dynamics is clearly non-integrable, but not fully chaotic as in the case considered in Ref. [54].

The positions of the resonances in the reflection and transmission spectra of a MB yield its eigenfrequencies f_n. They were measured by attaching antennas to the 10 ports and connecting them via a switch to a Keysight N5227A vector network analyzer (VNA) with Q086MMHF-0110CM-1L coaxial cables suitable for frequencies below 50 GHz. The VNA couples microwaves into the resonator via one antenna a and receives them at the same or another antenna b, and determines their relative amplitude $|S_{ba}|$ and phase ϕ_{ba}, yielding the S-matrix elements, $S_{ba} = |S_{ba}|\mathrm{e}^{\mathrm{i}\phi_{ba}}$. In the measurements performed at superconducting conditions the resonances were isolated in the considered frequency ranges and thus well described by the complex Breit–Wigner form, $S_{ba} = \delta_{ba} - \mathrm{i}\sqrt{\gamma_{na}\gamma_{nb}}/(f - f_n + (\mathrm{i}/2)\Gamma_n)$, with γ_{na} and γ_{nb} denoting the partial widths associated with antennas a and b and Γ_n the total resonance width, which is small since absorption into the walls of the MB is negligible at superconducting conditions. To identify the eigenfrequencies we fit the Breit–Wigner form to the resonances and thereby obtained complete sequences for both cavities for $B = 0$ mT and $B = 200$ mT.

In Fig. 2 measured transmission spectra are exhibited for the MB1 with short and long antennas for $B = 0$ mT and $B = 200$ mT. To facilitate comparison with other spectra black dashed vertical lines are plotted at the positions of the resonances of the MB1 with short antennas. Their comparison with those obtained with long antennas shows that they induce a perturbation which is strong enough to shift the positions of the resonances, that is, the eigenfrequencies. This is confirmed by the spectral properties exhibited below. Also the effect of magnetization is that the resonances for $B = 200$ mT are shifted with respect to those for $B = 0$ mT, which also becomes visible in a change of the spectral properties. To estimate the size of $\mathcal{T}$-invariance violation, we analyzed the violation of the principle of detailed balance, $|S_{ab}| = |S_{ba}|$, in terms of the measure[70] $\Delta_{ab} = (||S_{ab}| - |S_{ba}||)/(|S_{ab}| + |S_{ba}|)$. Here we used the non-calibrated S-matrix elements, because at superconducting conditions a special procedure is required, which is cumbersome.[109–112] Since we are only interested in spectral properties of the MBs, this procedure is not needed. Yet, we cannot get any information on the strength of $\mathcal{T}$-invariance violation from phase-dependent fluctuation properties of the S matrix, like the cross-correlation coefficients.[69,70] In Fig. 3 Δ_{ab} is plotted for the MB1 (left) and the MB2 (right). For $B = 0$ mT the principle of detailed balance is fulfilled up to experimental accuracy, whereas for $B = 200$ mT its size is similar for MB1 with short antennas and MB2 and slightly smaller for MB1 with long antennas.

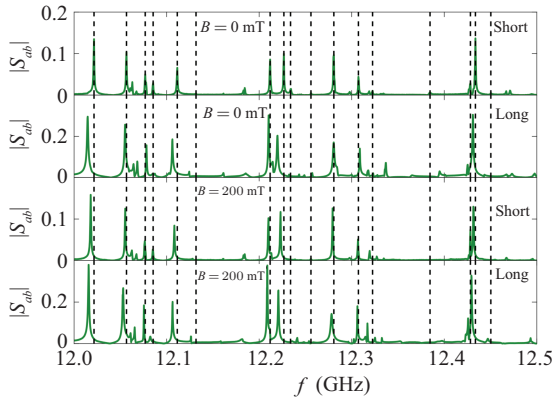


Fig. 2. Comparisons of the transmission spectra of the MB1 measured with short (first and third row) and long (second and fourth row) antennas at ≈ 5 K for external magnetic field $B = 0$ mT (first two rows) and $B = 200$ mT (last two rows). The black dashed vertical lines indicate the positions of the resonances of the MB1 with short antennas to facilitate the comparison with the other spectra.

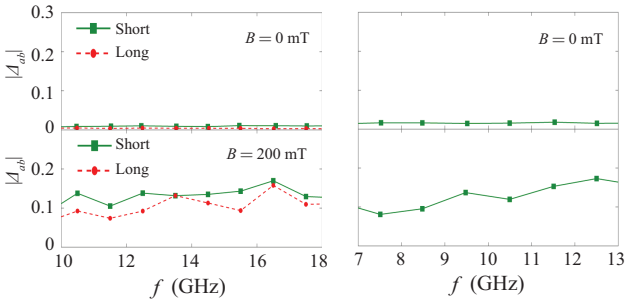


Fig. 3. Left: Relative size of the violation of the principle of detailed balance in the MB1 with short antennas (green squares) and long antennas (red dots) for $B = 0$ mT (top) and $B = 200$ mT (bottom). Right: Same as left panels for the MB2. Note that the symbols show the average values determined in 1 GHz windows.

3. The extended RP model

The RP model is a paradigmatic RMT model[47] which is applied to characterize the spectral properties of typical quantum systems, whose classical counterpart exhibits a mixed integrable-chaotic dynamics. These are predicted to exhibit a behavior intermediate between Poisson and WD statistics.

The model depends on a parameter λ which induces a transition from a random matrix which is diagonal to one from either of the WD ensembles, denoted as $\hat{H}_0$ and $\hat{H}^\beta$, respectively,

$$\hat{H}^{0\to\beta}(\lambda) = \hat{H}_0 + \Gamma_N \lambda \hat{H}^\beta, \quad \beta = 1,2,\ \Gamma_N = \frac{2\pi}{N}. \tag{1}$$

The probability density of the elements of $\hat{H}_0$ is arbitrary. We chose them as Gaussian distributed random numbers, where the variance equals that of the diagonal elements of $\hat{H}^\beta$, $\sigma_d^2 = \langle H_{nn}^2 \rangle = 1/(2\beta N)$ and that of the off-diagonal elements of $\hat{H}^\beta$ is $\sigma_{\rm off}^2 = \left\langle \left(H_{nm}^{(q)} \right)^2 \right\rangle = 1/(4\beta N)$. Here N denotes the dimension of $\hat{H}$ and $q = 0,\ldots,\beta-1$ counts the number of independent components of the off-diagonal matrix elements of $\hat{H}$. For $\beta = 1$, $\hat{H}^{0\to\beta}(\lambda)$ is real symmetric, whereas for $\beta = 2$ it is complex Hermitian. The scaling of λ, denoted by Γ_N is introduced to ensure that the spectral properties of the unfolded eigenvalues do not depend on the dimension of $\hat{H}^{0\to\beta}(\lambda)$.[2,77,81,113,114] We followed Ref. [114] and chose it equal to the inverse of the average density of the diagonal elements of $\hat{H}_0$; see Eq. (1). With increasing λ the matrix elements of $\hat{H}^\beta$ become dominant, implicating a transition of the spectral properties from Poisson to WD statistics.

Recently, we studied the transition from Poisson to GUE experimentally with an MB.[54] In this paper we analyze experimental data for cavities with the shapes of CBs whose dynamics is intermediate between integrable and chaotic and whose spectral properties agree with those of the RP model Eq. (1) with $\beta = 1$, subject to a non-vanishing external magnetic field applied to a ferrite which acts as a random potential and induces partial $\mathcal{T}$-invariance violation. The objective is to verify, whether such systems, or generally, typical quantum systems with these features are described by an extended RP model comprising random matrices given by

$$\hat{H}^{0\to1\to2}(\eta,\xi) = \hat{H}_0 + \Gamma_N \eta \hat{H}^{\beta=1} + \mathrm{i}\Gamma_N \xi \hat{H}^A, \quad \eta \geq \xi, \tag{2}$$

where $\hat{H}^A$ is antisymmetric with Gaussian distributed random numbers with zero mean and the same variances $\sigma_{\rm off}$, as in the RP model Eq. (1). Note, that equation (2) can be brought to the form

$$\hat{H}^{0\to1\to2}(\eta,\xi) = \frac{1}{2}\left[\hat{H}^{0\to1}(2\eta) + \hat{H}^{0\to2}(2\xi)\right]$$

with $\eta = \lambda + \xi$. To determine the sizes of chaoticity and of $\mathcal{T}$-invariance violation, we use the known Wigner-surmise like nearest-neighbor spacing distributions (NNSDs) for the RP model Eq. (1)[50,60,115,116] and derive a corresponding analytical expression for the RP model Eq. (2), which is validated with the experimental data. These analytical results are employed to identify the RMT model suitable for the description of the experimental data and to determine the parameters λ,η,ξ entering Eqs. (1) and (2). Based on the thus determined parameters and the corresponding RP model we then compute other statistical measures for short- and long-range correlations.

In Appendix B we derive an analytical expression for the Wigner-surmise like NNSD of the extended RP model Eq. (2),

$$P^{0\to1\to2}(s) = \frac{4\tilde{D}}{\sqrt{\pi}}\frac{\eta}{\xi}(\tilde{D}s)^2 \mathrm{e}^{-\Sigma(\tilde{D}s)^2} \int_0^\infty \mathrm{d}p \exp\left(-\frac{p^2}{8\eta^2} - p\right) \int_0^1 \mathrm{d}x \cosh\left[p\frac{\tilde{D}sx}{\sqrt{2}\eta}\right] \mathrm{e}^{(\tilde{D}sx)^2\Delta} I_0\left[(\tilde{D}s)^2\Delta(1-x^2)\right] \tag{3}$$

with

$$\Sigma = \frac{\eta^2+\xi^2}{2\xi^2}, \quad \Delta = \frac{\eta^2-\xi^2}{2\xi^2}, \tag{4}$$

and $\tilde{D} = D/(2\sqrt{2}\eta)$ with $D = \int_0^\infty \mathrm{d}s s P^{0\to1\to2}(s;\tilde{D} = 1/[2\sqrt{2}\eta])$. As outlined in the Appendix B, in the limits $\xi \to 0$ and $\xi \to \eta$ the results Eqs. (B1) and (B2) are recovered, respectively.

4. Analysis of correlations in the eigenfrequency spectra

For the analysis of spectral properties the sorted eigenfrequencies f_n, $f_n < f_{n+1}$ are unfolded to average spacing unity by replacing them by the smooth part of the integrated resonance density $\mathcal{N}^{\rm smooth}(f)$, $\varepsilon_n = \mathcal{N}^{\rm smooth}(f_n)$. For QBs and MBs with metallic walls it is given by Weyl's formula

$$\mathcal{N}^{\rm smooth}(f) = \frac{\mathcal{A}\pi}{c^2}f^2 - \frac{\mathcal{L}}{2c}f + N_0,$$

with $\mathcal{A}$ and $\mathcal{L}$ denoting the area and perimeter of the billiard, respectively, and it provides for $B = 0$ mT a good approximation for the cavities, which contain a ferrite disk instead of a metallic disk at the center. For $B \neq 0$ mT, $\mathcal{N}^{\rm smooth}(f)$ is obtained by fitting a quadratic polynomial to the experimentally determined $\mathcal{N}(f)$. The parameters λ, ξ, η of the RP models Eqs. (1) and (2) were determined in all considered cases by fitting the corresponding Wigner-surmise like approximation to the experimentally determined NNSD. Note, that the sizes of $\mathcal{T}$-invariance violation and chaoticity induced by the magnetized ferrite depend on frequency[69,97,117] wherefore we analyzed spectra in frequency windows, whose widths were chosen such that the size of chaoticity and of $\mathcal{T}$-invariance violation depend only weakly on frequency.

First, we applied the analytical result Eq. (3) for the NNSD of the RP model Eq. (2) to that of the eigenfrequencies of the MB1 with short antennas and $B = 200$ mT. The resulting curves are plotted as blue squares in the left part of

Fig. 4. They are compared with those obtained from the fit of the NNSD of the RP model Eq. (1) with $\beta = 2$ (red dots); see Ref. [54]. Here, we divided the eigenfrequency spectrum into the frequency windows given in the legends of the panel. The crucial difference between the RP models Eqs. (1) and (2) is, that in the former model the size of chaoticity and $\mathcal{T}$-invariance violation are characterized by one parameter ξ_L, whereas in the latter the effects inducing chaoticity and $\mathcal{T}$-invariance violation are described by two independent parameters η and ξ. The very good agreement between the red and blue curves and of the parameter values implies that, as assumed in Ref. [54], indeed the chaoticity and $\mathcal{T}$-invariance violation, that are induced by magnetizing the ferrite at the center of the cavity, are accounted for by one parameter ξ_L. This finding is confirmed in the right part of Fig. 4. There, we compare the experimental ratio distributions with the analytical Wigner-surmise like result for the RP model Eq. (1) for $\beta = 2$ given in Eq. (C1), which was derived by one of the authors (BD) in Ref. [95]. The parameters ξ_L resulting from the fit with Eq. (C1) to the experimental ratio distributions is similar to that obtained with Eq. (B2) for the NNSD and the agreement between theory and experiment is very good. We also show the experimental results for the eigenfrequency range 10 GHz–20 GHz. Using the whole frequency range is equivalent to superimposing spectra with different values of λ_L, ξ_L or η and ξ so that the fit yields averages over these parameters, as confirmed; see legends in the panels.

In Fig. 5 we compare the NNSDs obtained for the MB1 with 10 long antennas for $B = 0$ mT (left) and $B = 200$ mT (right) to the best fitting analytical curves obtained from Eq. (B1) (red dots in the left part), Eq. (B2) (red dots in the right part), and Eq. (3) (blue squares in the right part). Here, the spectra were divided into the frequency ranges comprising 257 eigenfrequencies. Note that similar to the singular MBs containing only one long antenna the size of the perturbation depends on the frequency. However, as indicated by the values of λ_L obtained from the fits, it seemingly barely changes in the frequency range from 10 GHz–16 GHz and differs only slightly from the one in the range from 16 GHz–18 GHz. These results imply, that indeed the spectral properties are intermediate between Poisson and GOE statistics for $B = 0$ mT, yet closer to Poisson than to WD statistics as confirmed by the comparatively small value of λ_L. This indicates that the classical dynamics is mixed regular-chaotic with a small chaotic component. As visible in the right figure, the best-fitting curves obtained with Eq. (B2) as fit function clearly differ from those obtained with Eq. (3). Furthermore, the agreement of the latter with the experimental curves is better than that for the former, as expected, because for $B = 0$ mT the dynamics is not fully integrable, as assumed in the RP model Eq. (1). The values of ξ_L are smaller than those for the measurements with short antennas, implying that $\mathcal{T}$-invariance violation is weaker in that case, in agreement with Fig 3. To verify the applicability of the RP model Eq. (2) we performed the random-matrix simulations to compute other statistical measures, for which analytical results are not available. We inserted the parameter values resulting from the fit of Eq. (3) into that equation and analyzed the Dyson–Mehta statistics $\Delta_3(L)$, that is the spectral rigidity,[8,118] which provides information on long-range correlations, and the distribution of ratios $r_n = (f_{n+1} - f_n)/(f_n - f_{n-1})$ of the non-unfolded eigenfrequencies.[119–121] As illustrated in Fig. 6, for both statistical measures the agreement between the experimentally determined curves and those obtained from the ensemble average of 200 400×400-dimensional random matrices of the form Eq. (2) is good.

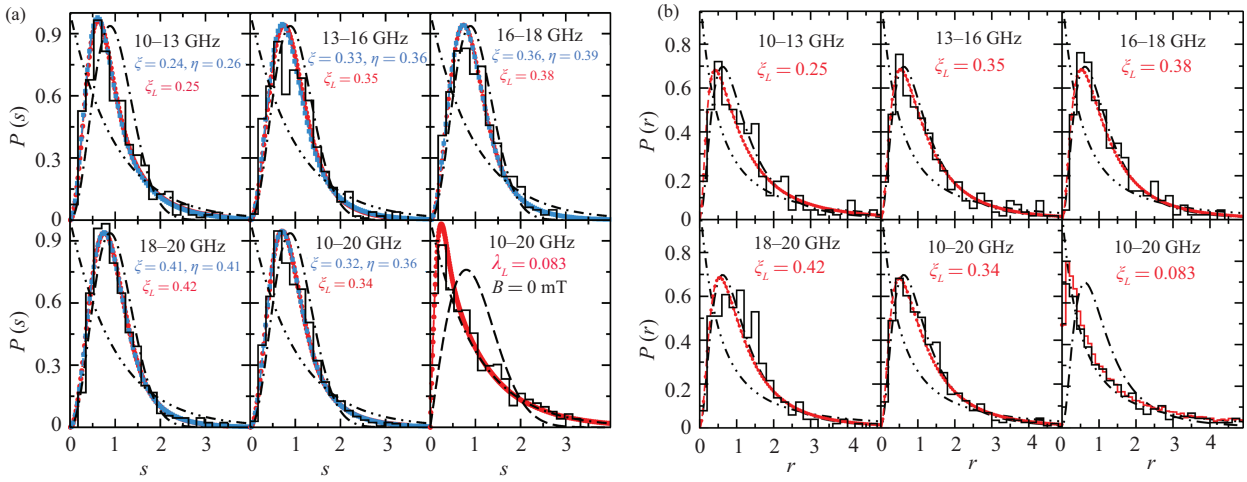


Fig. 4. (a) Nearest-neighbor spacing distributions. Shown are the experimental results for the MB1 for short antennas with $B = 0$ mT and $B = 200$ mT (black histograms). The red curves are obtained from a fit of the Wigner-surmise Eqs. (B1) and (B2) of the appendix to the experimental results with $B = 0$ mT and $B = 200$ mT, respectively, whereas the blue curves result from a fit of the Wigner-surmise Eq. (3). Shown are the results for 231 $f_n \in [10, 13]$ GHz, 294 $f_n \in [13, 16]$ GHz, 232 $f_n \in [16, 18]$ GHz, and 256 $f_n \in [18, 20]$ GHz, and for the whole considered frequency range, $f_n \in [10, 20]$ GHz. (b) Validation of the analytical result for the ratio distribution $P^{1\to 2}(r)$ given in Eq. (C1). Here, we used the values of ξ_L determined from the fits shown in the left panel. The dash–dot–dot, dashed and dash–dotted lines show the corresponding curves for Poisson, GOE and GUE statistics, respectively.

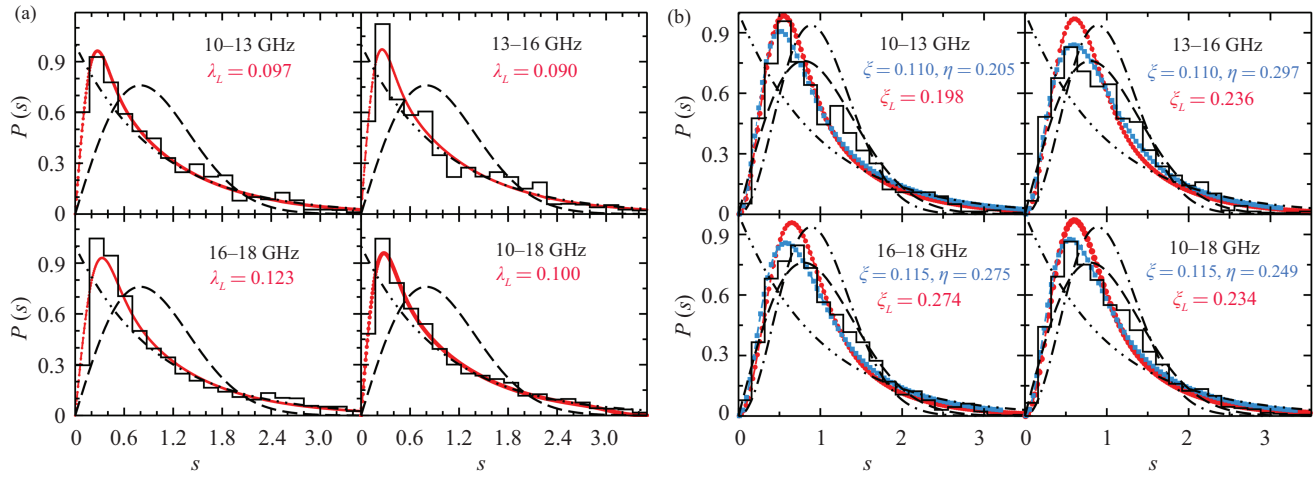


Fig. 5. Nearest-neighbor spacing distributions. Shown are the experimental results for the MB1 (black histograms) with long antennas for $B = 0$ mT (a) and $B = 200$ mT (b). Here, we chose the frequency intervals such that each of them contained 257 eigenfrequencies. The red curves are obtained from a fit of the Wigner-surmise Eqs. (B1) (left) and (B2) (right) to the experimental results, whereas the blue curves result from a fit of the Wigner-surmise Eq. (3). The dash–dot–dot, dashed and dash–dotted lines show the corresponding curves for Poisson, GOE, and GUE statistics, respectively.

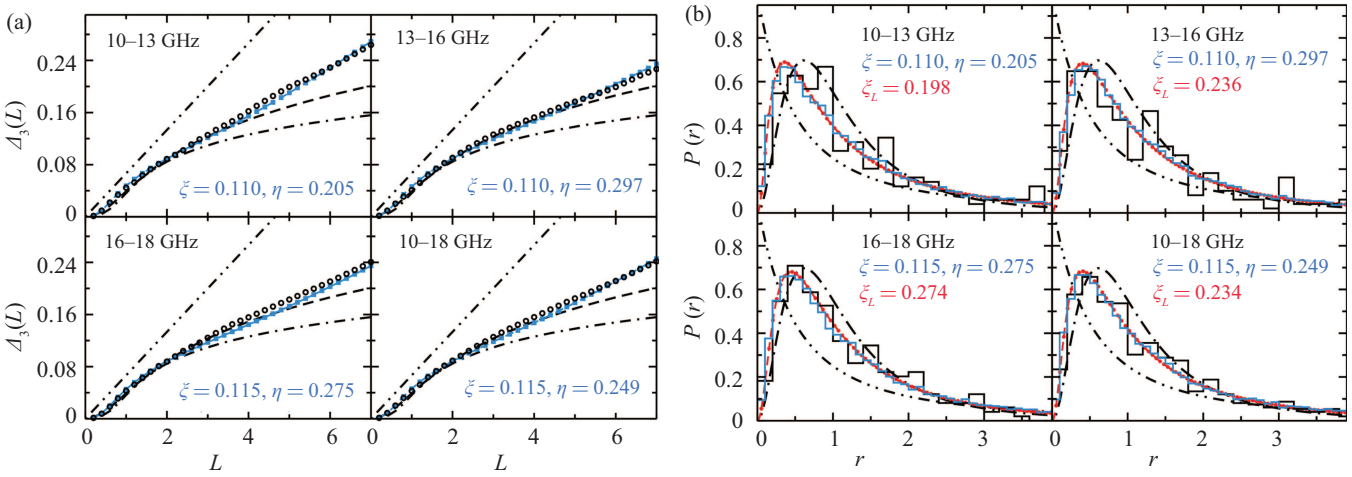


Fig. 6. (a) Dyson–Mehta statistics and (b) ratio distributions. Shown are the experimental results for the MB1 with long antennas (black circles and black histograms). The blue curves and red dots are obtained from an ensemble of random matrices of the form Eq. (2) and from Eq. (C1) using the values of ξ, η, and ξ_L, respectively, obtained from the fits in Fig. 5. The dash–dot–dot, dashed- and dash–dotted lines show the corresponding curves for Poisson, GOE, and GUE statistics, respectively.

In the right figure we also show the curves computed from Eq. (C1) using the values of ξ_L obtained from the fit with Eq. (B2). In contrast to the NNSDs, the ratio distributions of the RP models (1) and (2) barely differ. This implies, that the NNSD is more sensitive to slight perturbations, i.e., in the present case to differences between η and ξ, than the ratio distribution, thus confirming the observations made in Ref. [95]. Consequently, the Wigner-surmise like NNSD is a more appropriate tool for the determination of the size of chaoticity and $\mathcal{T}$ invariance than the ratio distribution.

In Fig. 7 the NNSDs of the MB2 with $B = 0$ mT (left) and $B = 200$ mT (right) are exhibited. In this case the spectral properties are closer to WD statistics than to Poisson statistics in both cases. Furthermore, the curves obtained from Eq. (B2) (red dots) differ considerably from those deduced from Eq. (3) (blue squares), and the latter agree well with the experimental results. Note, that in this case the perturbation induced by the two scatterers is stronger than that due to the long antennas, so that the chaotic component is already large for $B = 0$ mT. The sizes of the parameter ξ_L are comparable to those for the MB1 with short antennas, thus confirming the results in Fig. 3. We again verify the applicability of the RP model Eq. (2) by performing random-matrix simulations. Comparing the Dyson–Mehta statistics and ratio distributions for the values of η and ξ obtained from the fits employing Eq. (3) to the corresponding experimental results yields a good agreement as demonstrated in Fig. 8. Similar to the results obtained for the MB1 with long antennas, the ratio distributions obtained with the RP model Eq. (1) are barely distinguishable from those resulting from the model Eq. (2), thus confirming our previous conclusion that they are not suitable for the determination of the size of chaoticity and $\mathcal{T}$-invariance violation.

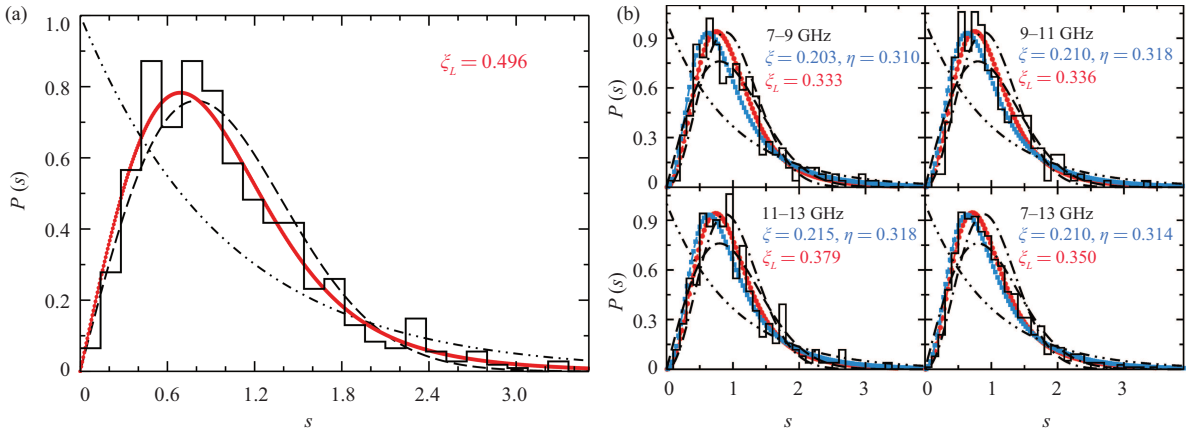


Fig. 7. Same as Fig. 5 but for the MB2.

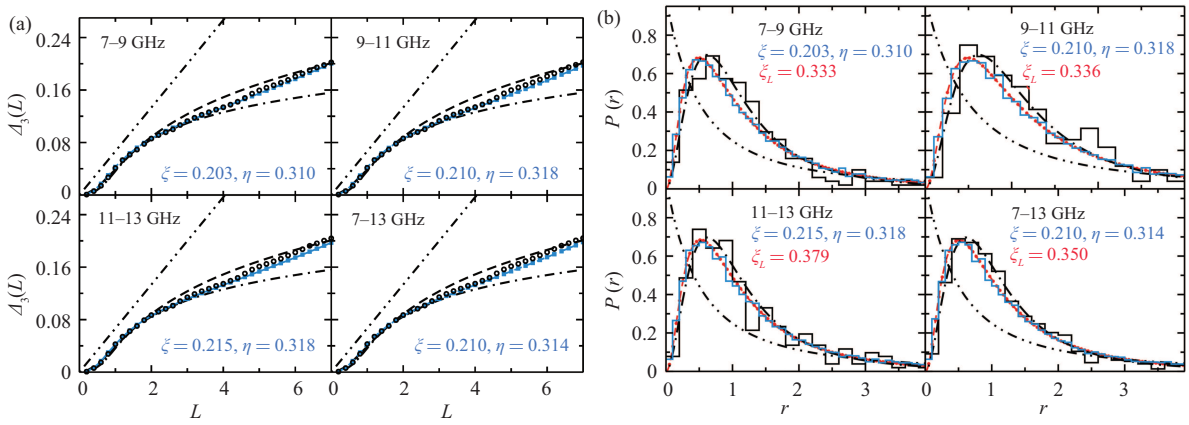


Fig. 8. Same as Fig. 6 but for the MB2.

5. Conclusions

We propose a procedure to determine the size of chaoticity and $\mathcal{T}$-invariance violation of typical quantum systems whose classical dynamics experiences a transition from mixed regular-chaotic to fully chaotic with complete $\mathcal{T}$-invariance violation. It involves an extended RP model proposed in this paper and the Wigner-surmise like analytical result for the corresponding NNSD, whose derivation is provided in the appendix. This procedure is verified with experimental data obtained by inducing in MBs, whose top and bottom plates are made from niobium, a superconductor of type II,[74] and whose spectral properties are between Poisson and GOE and well described by the RP model Eq. (1) with $\beta = 1$, $\mathcal{T}$-invariance violation with a ferrite, that is magnetized with an external magnetic field B. The experiments were performed at superconducting conditions, thereby achieving high-quality factors even for nonzero magnetic field B, a prerequisite to facilitate the identification of a complete sequence of ~ 1000 eigenfrequencies. Accordingly, we were able to analyze the spectral properties in various frequency ranges containing about 250 eigenfrequencies and to study the gradual transition from spectral statistics between Poisson and GOE to GUE. To validate the proposed procedure we computed for the thus determined parameter values long-range correlations, for which no analytical results are available, for the experimental data and the RMT model Eq. (2) and found good agreement between them. Furthermore, we experimentally verify with the data for the MB1 with short antennas an analytical expression for the ratio distribution of the RP model Eq. (1), derived by one of the co-authors in Ref. [95].

Acknowledgements

Project supported by the National Natural Science Foundation of China (Grant Nos. 11775100, 12247101, and 11961131009), Xiaodong Zhang acknowledges the financial support from the China Scholarship Council (Grant No. CSC-202306180087), and Barbara Dietz and Xiaodong Zhang acknowledge the financial support from the Institute for Basic Science in Korea (Grant No. IBS-R024-D1). We thank Sheng Xue Zhang who helped with the design of the niobium parts.

Appendix A: Length spectra

The modulus of the Fourier transform of the fluctuating part of the spectral density from wave number to length yields

a length spectrum. It has this name because it exhibits peaks at the lengths of the periodic orbits of the corresponding classical system.

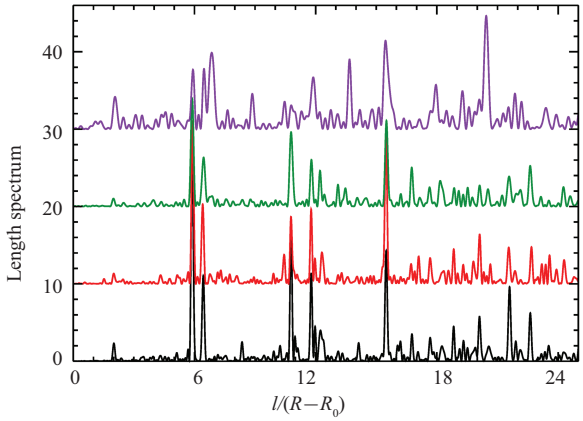


Fig. A1. Length spectra for $B = 0$ mT for, from bottom to top, the ring QB (black solid line), the MB1 for short (red solid line) and long (green solid lines) antennas, and the MB2 (violet solid line). Here, $R = 250$ mm denotes the radius of the circle billiard and $R_0 = 30$ mm the radius of the ferrite disk at its center. At lengths corresponding to orbits, that hit the ferrite disk and thus feel the differing BCs, the length spectra of the MB1 with short and long antennas differ.[54]

In Fig. A1 are exhibited from bottom to top the length spectra for the ring QB, for the MB1 with short and long antennas and for the MB2. The length spectra of the QB and MB1 with short antennas mainly differ at lengths that correspond to orbits that hit the inner billiard wall and the ferrite disk, respectively. This is attributed to the differing BCs at these walls, namely mixed Dirichlet and Neumann BCs for the MB, implying that there is no specular (hard-wall) reflection at the ferrite-disk wall in the ray-dynamical limit.[54] The length spectrum for the MB1 with long antennas clearly differs from that with short antennas, as it shows additional peaks that may be attributed to orbits that hit the antennas.[107,122,123]

Appendix B: Wigner-surmise like approximations for the RP model Eq. (1)

The Wigner-surmise like approximations for the NNSD of random matrices from the WD ensembles and the RP model Eq. (1) have been derived based on 2×2-dimensional random matrices. For the case $\beta = 1$ in Eq. (1) it is given by[50]

$$P^{0\to 1}(s;\tilde{D}) = 2\tilde{D}^2 s\,\mathrm{e}^{-(\tilde{D}s)^2}\int_0^\infty \mathrm{d}p \exp\left(-\frac{p^2}{8\lambda_L^2}-p\right)\mathrm{I}_0\left(\frac{\tilde{D}sp}{\sqrt{2}\lambda_L}\right), \tag{B1}$$

where $\tilde{D} = D/(2\sqrt{2}\lambda_L)$ with

$$D = \int_0^\infty \mathrm{d}s s P^{0\to 1}(s;\tilde{D}=1/[2\sqrt{2}\lambda_L]),$$

and $\mathrm{I}_0(x)$ is the modified Bessel function. The distribution experiences a transition from Poisson for $\lambda_L = 0$ to the Wigner surmise for $\beta = 1$ for $\lambda_L \to \infty$. In Ref. [60] the corresponding Wigner-surmise like approximation was derived for the case $\beta = 2$ in Eq. (1),

$$P^{0\to 2}(s;\tilde{D}) = \frac{4\tilde{D}}{\sqrt{\pi}}(\tilde{D}s)^2\,\mathrm{e}^{-(\tilde{D}s)^2}\int_0^\infty \mathrm{d}p \exp\left(-\frac{p^2}{8\xi_L^2}-p\right)\frac{\sinh z}{z}, \tag{B2}$$

where $\tilde{D} = D/(2\sqrt{2}\xi_L)$ with

$$D = \int_0^\infty \mathrm{d}s s P^{0\to 2}(s;\tilde{D}=1/[2\sqrt{2}\xi_L])$$

and $z = p\tilde{D}s/\sqrt{2}\xi_L$. The proof that these distributions approach the corresponding WD surmise for $\lambda_L \to \infty$ and $\xi_L \to \infty$, respectively is straightforward. The Poisson distribution is recovered for $\lambda_L \to 0$ and $\xi_L \to 0$ employing that

$$\frac{1}{\alpha}\exp\left(-\frac{x^2}{\alpha^2}\right) \xrightarrow{\alpha\to 0} \sqrt{\pi}\delta(x),$$

where the limits have to be taken such that $\lambda_L < s$ or $\xi_L < s$, respectively.

We verified the scaling of the parameters λ_L and ξ_L, which differ by a factor of $\sqrt{2}$ from those given in Refs. [50, 60,103,115,116], by comparing $P^{0\to\beta}(s;D)$ to ensemble averages of the NNSD of the eigenvalues of 200 $N\times N$-dimensional random matrices with $N = 400, 800, 1200$ of the form $\hat{H}^{0\to\beta}(\lambda)$ in Eq. (1). This yielded that the analytical and numerical distributions agree well for $\lambda = \lambda_L$ and $\lambda = \xi_L$ for $\beta = 1$ and $\beta = 2$, respectively. The discrepancy to previous results[50,54,60,95] originates from the scaling Γ_N of λ introduced in Eq. (1).

Appendix C: The ratio distribution for the transition from $\beta = 0 \to 2$

Based on the joint probability distribution of the eigenvalues of $\hat{H}^{0\to 2}(\lambda)$ for the transition from Poisson to GUE[60,81,82,124] one of the authors (BD) derived in Ref. [95] a Wigner-surmise like analytical expression for the ratio distribution,

$$P^{0\to 2}(r) = \frac{r(r+1)}{R^3}\frac{1}{2\pi}\left\{\sqrt{3}\frac{\lambda^2}{\lambda^2+1}\frac{(3R-2)}{2R} + (2+r)\lambda^2\int_{-\pi}^{\pi}\frac{\mathrm{d}\varphi}{\sin\varphi}\left(-X_1+\frac{2}{X_1}+\frac{1}{3X_1^3}\right)\left[1-\frac{2}{\pi}\arctan(X_1)\right]\right.$$

$$+(1+2r)\lambda^2\int_{-\pi}^{\pi}\frac{\mathrm{d}\varphi}{\sin\varphi}\left(-X_2+\frac{2}{X_2}+\frac{1}{3X_2^3}\right)\left[1-\frac{2}{\pi}\arctan(X_2)\right]$$
$$+\frac{2}{\pi}\lambda^2\int_{-\pi}^{\pi}\frac{\mathrm{d}\varphi}{\sin\varphi}\left[\frac{2+r}{3}\frac{1}{X_1^2(1+X_1^2)}+\frac{1+2r}{3}\frac{1}{X_2^2(1+X_2^2)}\right]\Bigg\}, \tag{C1}$$

where $X_i=\sqrt{A_i(\varphi)}/F_i(\varphi)$, $i=1,2$ with

$$A_i(\varphi)=\frac{2}{3}(\alpha^2+1)\left(1-\frac{\sin\varphi}{2}\right)-F_i^2(\varphi), \tag{C2}$$

$$F_1(\varphi)=\frac{1}{3\sqrt{R}}\left|(2+r)\cos(\varphi/2)+(r-1)\sin(\varphi/2)\right|, \tag{C3}$$

$$F_2(\varphi)=\frac{1}{3\sqrt{R}}\left|(r-1)\cos(\varphi/2)+(1+2r)\sin(\varphi/2)\right|, \tag{C4}$$

and $R=(2/3)(1+r+r^2)$. It is proven there that

$$P^{0\to2}(r)\xrightarrow{\lambda\to0}\frac{3\sqrt{3}}{2\pi(1+r+r^2)}, \tag{C5}$$

which is the ratio distribution for the eigenvalues of a 3×3-dimensional diagonal matrix with Gaussian distributed entries, and

$$P(r)\xrightarrow{\lambda\to\infty}\frac{81\sqrt{3}}{4\pi}\frac{[r(1+r)]^2}{(1+r+r^2)^4}, \tag{C6}$$

which is the ratio distribution for the Wigner-surmise like analytical result for the GUE. Note, that in the derivation the matrix elements of the diagonal matrix H_0 in Eq. (1) were chosen as Gaussian distributed matrix elements, as in the numerical simulations; see below Eq. (1). More information can be found in Ref. [95].

Appendix D: The NNSD for the transition from $\beta=0\to1\to2$

A Wigner-surmise like expression for the NNSD of random matrix describing the transition from Poisson to GOE and then to GUE, experienced when exposing it to $\mathcal{T}$-invariance violation, is obtained based on 2×2 random matrices of the form Eq. (2),

$$\hat{H}^{0\to1\to2}=\begin{pmatrix}0&0\\0&p\end{pmatrix}+\tilde{\eta}\begin{pmatrix}h_{11}&h_{12}\\h_{12}&h_{22}\end{pmatrix}+\tilde{\xi}\begin{pmatrix}0&\mathrm{i}\varepsilon\\-\mathrm{i}\varepsilon&0\end{pmatrix}=\begin{pmatrix}A&B\\B^*&C\end{pmatrix} \tag{D1}$$

with $\tilde{\eta}=\sqrt{2}\eta$, $\tilde{\xi}=\sqrt{2}\xi$, $A=\eta h_{11}$, $B=B_1+\mathrm{i}B_2$ where $B_1=\tilde{\eta}h_{12}$, $B_2=\tilde{\xi}\varepsilon$, and $C=p+\eta h_{22}$. Here, the factor $\sqrt{2}$ accounts for the scaling Γ_N in Eq. (2), for which the parameters λ_L, ξ_L, η, ξ measure the size of the parameters in units of the inverse of the average density of the entries of H_0. Furthermore, we transformed the matrix H_0, whose elements p_1,p_2 are uncorrelated random numbers, to one which only depends on the non-negative spacing p between them.[116] Its probability density is given as $P_0(p)=\mathrm{e}^{-p}$. Furthermore, h_{11}, h_{22}, and h_{12}, ε are Gaussian-distributed random numbers with zero mean and variance 1 and $1/\sqrt{2}$, respectively, yielding for the distributions of A, B, and C

$$p(A)=\frac{\mathrm{e}^{-A^2/2\sigma_2}}{\sqrt{2\pi\sigma_2}},\qquad p(B_1)=\frac{\mathrm{e}^{-B_1^2/\sigma_2}}{\sqrt{\pi\sigma_2}},\qquad p(B_2)=\frac{\mathrm{e}^{-B_2^2/\sigma_3}}{\sqrt{\pi\sigma_3}}, \tag{D2}$$

$$p(C)=\frac{\mathrm{e}^{-C^2/2\sigma_2}}{\sqrt{2\pi\sigma_2}}\int_0^\infty\mathrm{d}p\,\mathrm{e}^{-p^2/2\sigma_2}\exp\left[-p\left(1-\frac{C}{\sigma_2}\right)\right], \tag{D3}$$

where we introduced $\sigma_2=2\eta^2$, $\sigma_3=2\xi^2$. Then the NNSD $P^{0\to1\to2}(s)$ is obtained by computing the ensemble averages of the matrix elements of random matrices under the condition that the spacing of the eigenvalues

$$E_\pm=\frac{A+C}{2}\pm\frac{1}{2}\sqrt{(A-C)^2+4|B|^2}$$

of $\hat{H}^{0\to1\to2}$ is $s=\sqrt{(A-C)^2+4|B|^2}$,

$$\tilde{P}^{0\to1\to2}(s)=\frac{1}{2\pi^2\sigma_2\sqrt{\sigma_2\sigma_3}}\int_0^\infty\mathrm{d}p\,\mathrm{e}^{-p^2/2\sigma_2-p}\int_{-\infty}^\infty\mathrm{d}A\,\mathrm{e}^{-A^2/2\sigma_2}\int_{-\infty}^\infty\mathrm{d}C\,\mathrm{e}^{-C^2/2\sigma_2+pC/\sigma_2}$$
$$\times\int_{-\infty}^\infty\mathrm{d}B_1\,\mathrm{e}^{-B_1^2/\sigma_2}\int_{-\infty}^\infty\mathrm{d}B_2\,\mathrm{e}^{-B_2^2/\sigma_3}\delta\left(s-\sqrt{(A-C)^2+4(B_1^2+B_2^2)}\right). \tag{D4}$$

To perform the integrals over B_1 and B_2 we introduce polar coordinates, $B_1=\rho\cos\phi$, $B_2=\rho\sin\phi$ and obtain for the integrals in Eq. (D4)

$$\int_{-\infty}^\infty\mathrm{d}B_1\int_{-\infty}^\infty\mathrm{d}B_2\{\cdots\}\longrightarrow\frac{s}{2}\Theta(s-|A-C|)\int_0^\pi\mathrm{d}\phi\,\mathrm{e}^{-\Sigma[s^2-(A-C)^2]/4\sigma_2}\,\mathrm{e}^{\Delta\cos\phi[s^2-(A-C)^2]/4\sigma_2}, \tag{D5}$$

with

$$\Sigma = \frac{\sigma_2+\sigma_3}{2\sigma_3} = \frac{\eta^2+\xi^2}{2\xi^2}, \qquad \Delta = \frac{\sigma_2-\sigma_3}{2\sigma_3} = \frac{\eta^2-\xi^2}{2\xi^2}. \tag{D6}$$

Next, we introduce the variable $\tilde{A} = (A-C)$ and perform the integral over C yielding

$$\tilde{P}^{0\to1\to2}(s) = \frac{s^2}{2\sigma_2\sqrt{\pi\sigma_3}}\int_0^\infty \mathrm{d}p\,\mathrm{e}^{-p^2/4\sigma_2-p}\int_0^1 \mathrm{d}x\,\mathrm{e}^{-(sx)^2/4\sigma_2}\cosh\left[x\frac{sp}{2\sigma_2}\right]\mathrm{e}^{-(1-x^2)\Sigma s^2/4\sigma_2}\,\mathrm{I}_0\left(\frac{s^2}{4\sigma_2}\Delta(1-x^2)\right). \tag{D7}$$

Rescaling to average spacing unity yields the distribution Eq. (3),

$$P^{0\to1\to2}(s) = \frac{4\tilde{D}}{\sqrt{\pi}}\frac{\eta}{\xi}(\tilde{D}s)^2\,\mathrm{e}^{-\Sigma(\tilde{D}s)^2}\int_0^\infty \mathrm{d}p\exp\left(-\frac{p^2}{8\eta^2}-p\right)\int_0^1 \mathrm{d}x\cosh\left[p\frac{\tilde{D}sx}{\sqrt{2}\eta}\right]\mathrm{e}^{(\tilde{D}sx)^2\Delta}I_0\left((\tilde{D}s)^2\Delta(1-x^2)\right) \tag{D8}$$

with $\tilde{D} = D/(2\sqrt{2}\eta)$, where

$$D = \int_0^\infty \mathrm{d}s s P^{0\to1\to2}(s;\tilde{D} = 1/[2\sqrt{2}\eta]).$$

In the limit $\xi\to\eta$, that is, $\Sigma\to1$ and $\Delta\to0$ $\mathrm{I}_0\left((\tilde{D}s)^2\Delta(1-x^2)\right)\xrightarrow{\Delta\to0}1$ so the integral over x can be performed and the result for $P^{0\to2}(s)$ in Eq. (D2 is recovered. For $\xi\to0$ the integral (D5 becomes with the notation $x=(A-C)/s$

$$\begin{aligned}&\frac{1}{\sqrt{\pi}\xi}\int_{-\infty}^\infty \mathrm{d}B_1\int_{-\infty}^\infty \mathrm{d}B_2\{\cdots\}\xrightarrow{\xi\to0}\frac{s}{2}\Theta(1-|x|)\int_0^\pi \mathrm{d}\phi\exp\left\{-s^2\frac{(1-x^2)}{8\eta^2}\cos^2\left[\frac{\phi}{2}\right]\right\}\delta\left(s\frac{\sqrt{1-x^2}}{2}\sin\left[\frac{\phi}{2}\right]\right)\\ &=\frac{2\Theta(1-|x|)}{\sqrt{1-x^2}}\exp\left(-s^2\frac{(1-x^2)}{8\eta^2}\right),\end{aligned} \tag{D9}$$

yielding

$$\begin{aligned}&\tilde{P}^{0\to1\to2}(s)\xrightarrow{\xi\to0}\frac{s}{4\pi\eta^2}\mathrm{e}^{-s^2/8\eta^2}\int_0^\infty \mathrm{d}p\,\mathrm{e}^{-p^2/8\eta^2-p}\int_0^1\frac{\mathrm{d}x}{\sqrt{1-x^2}}2\cosh\left[x\frac{sp}{4\eta^2}\right]\\ &=\frac{s}{4\eta^2}\mathrm{e}^{-s^2/8\eta^2}\int_0^\infty \mathrm{d}p\,\mathrm{e}^{-p^2/8\eta^2-p}\,\mathrm{I}_0\left(\frac{sp}{4\eta^2}\right),\end{aligned} \tag{D10}$$

which turns into the results for the transition from Poisson to GOE after rescaling the spacings s to mean spacing unity.

References

[1] Giannoni M, Voros A and Zinn-Justin J (eds) 1989 *Chaos and Quantum Physics* (Amsterdam: Elsevier)
[2] Guhr T, Müller-Groeling A and Weidenmüller H A 1998 *Phys. Rep.* **299** 189
[3] Haake F, Gnutzmann S and Kuś M 2018 *Quantum Signatures of Chaos* (Heidelberg: Springer-Verlag)
[4] Berry M V and Tabor M 1977 *J. Phys. A* **10** 371
[5] Berry M 1979 *Structural Stability in Physics* (Berlin: Pergamon Press)
[6] Casati G, Valz-Gris F and Guarnieri I 1980 *Lett. Nuovo Cimento* **28** 279
[7] Bohigas O, Giannoni M J and Schmit C 1984 *Phys. Rev. Lett.* **52** 1
[8] Mehta M L 1990 *Random Matrices* (London: Academic Press)
[9] Porter C E 1965 *Statistical Theories of Spectra: Fluctuations* (New York: Academic)
[10] Brody T A, Flores J, French J B, Mello P A, Pandey A and Wong S S M 1981 *Rev. Mod. Phys.* **53** 385
[11] Zimmermann T, Köppel H, Cederbaum L S, Persch G and Demtröder W 1988 *Phys. Rev. Lett.* **61** 3
[12] Guhr T and Weidenmüller H A 1989 *Ann. Phys.* **193** 472
[13] Mehta M L 2004 *Random Matrices* (Amsterdam: Elsevier)
[14] Weidenmüller H and Mitchell G 2009 *Rev. Mod. Phys.* **81** 539
[15] Gómez J, Kar K, Kota V, Molina R, Relaño A and Retamosa J 2011 *Phys. Rep.* **499** 103
[16] Frisch A, Mark M, Aikawa K, Ferlaino F, Bohn J L, Makrides C, Petrov A and Kotochigova S 2014 *Nature* **507** 474
[17] Mur-Petit J and Molina R A 2015 *Phys. Rev. E* **92** 042906
[18] Dietz B, Heusler A, Maier K H, Richter A and Brown B A 2017 *Phys. Rev. Lett.* **118** 012501
[19] Naubereit P, Studer D, Viatkina A V, Buchleitner A, Dietz B, Flambaum V V and Wendt K 2018 *Phys. Rev. A* **98** 022506
[20] Wigner E P 1951 *Proc. Cambridge Phil Soc.* **47** 790
[21] Wigner E P 1955 *Ann. Math.* **62** 548
[22] Wigner E P 1957 *Ann. Math.* **65** 203
[23] Dietz B, Brown B A, Gayer U, Pietralla N, Ponomarev V Y, Richter A, Ries P C and Werner V 2018 *Phys. Rev. C* **98** 054314
[24] Sinai Y G 1970 *Russ. Math. Surv.* **25** 137
[25] Lazutkin V F 1973 *Math. USSR Izv.* **37** 186
[26] Bunimovich L A 1979 *Commun. Math. Phys.* **65** 295
[27] Berry M V 1981 *Eur. J. Phys.* **2** 91
[28] Wojtowski M 1986 *Comm. Math. Phys.* **105** 391
[29] Stöckmann H J and Stein J 1990 *Phys. Rev. Lett.* **64** 2215
[30] Sridhar S 1991 *Phys. Rev. Lett.* **67** 785
[31] Gräf H D, Harney H L, Lengeler H, Lewenkopf C H, Rangacharyulu C, Richter A, Schardt P and Weidenmüller H A 1992 *Phys. Rev. Lett.* **69** 1296
[32] Stein J and Stöckmann H J 1992 *Phys. Rev. Lett.* **68** 2867
[33] So P, Anlage S M, Ott E and Oerter R 1995 *Phys. Rev. Lett.* **74** 2662
[34] Deus S, Koch P M and Sirko L 1995 *Phys. Rev. E* **52** 11465
[35] Dietz B and Richter A 2015 *Chaos* **25** 097601
[36] Hul O, Bauch S, Pakoński P, Savytskyy N, Życzkowski K and Sirko L 2004 *Phys. Rev. E* **69** 056205
[37] awniczak M, Bauch S, Hul O and Sirko L 2010 *Phys. Rev. E* **81** 046204

[38] Hul O, Ławniczak M, Bauch S, Sawicki A, Kuś M and Sirko L 2012 *Phys. Rev. Lett.* **109** 040402
[39] Allgaier M, Gehler S, Barkhofen S, Stöckmann H J and Kuhl U 2014 *Phys. Rev. E* **89** 022925
[40] Białous M, Yunko V, Bauch S, Ławniczak M, Dietz B and Sirko L 2016 *Phys. Rev. Lett.* **117** 144101
[41] Rehemanjiang A, Allgaier M, Joyner C H, Müller S, Sieber M, Kuhl U and Stöckmann H J 2016 *Phys. Rev. Lett.* **117** 064101
[42] Rehemanjiang A, Richter M, Kuhl U and Stöckmann H J 2018 *Phys. Rev. E* **97** 022204
[43] Martínez-Argöello A M, Rehemanjiang A, Martínez-Mares M, Méndez-Bermúdez J A, Stöckmann H J and Kuhl U 2018 *Phys. Rev. B* **98** 075311
[44] Rehemanjiang A, Richter M, Kuhl U and Stöckmann H J 2020 *Phys. Rev. Lett.* **124** 116801
[45] Lu J, Che J, Zhang X and Dietz B 2020 *Phys. Rev. E* **102** 022309
[46] Che J, Lu J, Zhang X, Dietz B and Chai G 2021 *Phys. Rev. E* **103** 042212
[47] Rosenzweig N and Porter C 1960 *Phys. Rev.* **120** 1698
[48] Brody T A 1973 *Lett. Nuovo Cimento* **7** 482
[49] Berry M V and Robnik M 1984 *J. Phys. A* **17** 2413
[50] Lenz G and Haake F 1991 *Phys. Rev. Lett.* **67** 1
[51] Kota V K B 2014 *Embedded Random Matrix Ensembles in Quantum Physics* (Heidelberg: Springer-Verlag)
[52] Dumitriu I and Edelman A 2002 *J. Math. Phys.* **43** 5830
[53] Dumitriu I and Edelman A 2006 *J. Math. Phys.* **47** 063302
[54] Zhang X, Zhang W, Che J and Dietz B 2023 *Phys. Rev. E* **108** 044211
[55] Stöckmann H J 2000 *Quantum Chaos: An Introduction* (Cambridge: Cambridge University Press)
[56] Richter A 1999 *Playing billiards with microwaves — quantum manifestations of classical chaos Emerging Applications of Number Theory, The IMA Volumes in Mathematics and its Applications* Vol. 109 ed. Hejhal D A, Friedman J, Gutzwiller M C and Odlyzko A M (New York: Springer) p. 479
[57] Dietz B and Richter A 2019 *Phys. Scr.* **94** 014002
[58] Bohigas O, Giannoni M J, de Almeidaz A M O and Schmit C 1995 *Nonlinearity* **8** 203
[59] Pandey A and Shukla P 1991 *J. Phys. A* **24** 3907
[60] Lenz G 1992 *Zufallsmatrixtheorie und Nichtgleichgewichtsprozesse der Niveaudynamik*, Ph.D. thesis (Fachbereich Physik der Universität-Gesamthochschule Essen)
[61] Pluhař Z, Weidenmüller H A, Zuk J, Lewenkopf C and Wegner F 1995 *Ann. Phys.* **243** 1
[62] Guhr T 1996 *Ann. Phys.* **250** 145
[63] French J B, Kota V K B, Pandey A and Tomsovic S 1985 *Phys. Rev. Lett.* **54** 2313
[64] Mitchell G E, Richter A and Weidenmüller H A 2010 *Rev. Mod. Phys.* **82** 2845
[65] Aßmann M, Thewes J, Fröhlich D and Bayer M 2016 *Nat. Mater.* **15** 741
[66] Stoffregen U, Stein J, Stöckmann H J, Kuś M and Haake F 1995 *Phys. Rev. Lett.* **74** 2666
[67] Wu D H, Bridgewater J S A, Gokirmak A and Anlage S M 1998 *Phys. Rev. Lett.* **81** 2890
[68] Dietz B, Friedrich T, Metz J, Miski-Oglu M, Richter A, Schäfer F and Stafford C A 2007 *Phys. Rev. E* **75** 027201
[69] Dietz B, Friedrich T, Harney H L, Miski-Oglu M, Richter A, Schäfer F, Verbaarschot J and Weidenmüller H A 2009 *Phys. Rev. Lett.* **103** 064101
[70] Dietz B, Friedrich T, Harney H L, Miski-Oglu M, Richter A, Schäfer F and Weidenmüller H A 2010 *Phys. Rev. E* **81** 036205
[71] Meissner W and Ochsenfeld R 1933 *Die Naturwissenschaften* **21** 787
[72] Onnes H K 1911 *Further Experiments with Liquid Helium. G. On the Electrical Resistance of Pure Metals, etc. VI. On the Sudden Change in the Rate at which the Resistance of Mercury Disappears* (Comm. from the Phys. Lab., Leiden, 1911)
[73] Dietz B, Klaus T, Miski-Oglu M, Richter A and Wunderle M 2019 *Phys. Rev. Lett.* **123** 174101
[74] Shubnikov L V, Ehotkevich V I, Shepelev Y D and Riabinin Y N 1937 *Zh. Eksper. Teor. Fiz.* **7** 221
[75] French J, Kota V, Pandey A and Tomsovic S 1988 *Ann. Phys.* **181** 235
[76] Leyvraz F and Seligman T H 1990 *J. Phys. A: Math. Gen.* **23** 1555
[77] Pandey A 1995 *Chaos, Solitons and Fractals* **5** 1275
[78] Brézin E and Hikami S 1996 *Nucl. Phys. B* **479** 697
[79] Guhr T 1996 *Phys. Rev. Lett.* **76** 2258
[80] Altland A and Zirnbauer M R 1997 *Phys. Rev. B* **55** 1142
[81] Kunz H and Shapiro B 1998 *Phys. Rev. E* **58** 400
[82] Frahm K M, Guhr T and Müller-Groeling A 1998 *Ann. Phys.* **270** 292
[83] Kravtsov V E, Khaymovich I M, Cuevas E and Amini M 2015 *New J. Phys.* **17** 122002
[84] Facoetti D, Vivo P and Biroli G 2016 *Europhys. Lett.* **115** 47003
[85] Truong K and Ossipov A 2016 *Europhys. Lett.* **116** 37002
[86] Monthus C 2017 *J. Phys. A: Math. Theor.* **50** 295101
[87] von Soosten P and Warzel S 2019 *Lett. Math. Phys.* **109** 905
[88] Pino M, Tabanera J and Serna P 2019 *J. Phys. A: Math. Theor.* **52** 475101
[89] Tomasi G D, Amini M, Bera S, Khaymovich I M and Kravtsov V E 2019 *SciPost Phys.* **6** 014
[90] Bogomolny E and Sieber M 2018 *Phys. Rev. E* **98** 032139
[91] Berkovits R 2020 *Phys. Rev. B* **102** 165140
[92] Khaymovich I M, Kravtsov V E, Altshuler B L and Ioffe L B 2020 *Phys. Rev. Res.* **2** 043346
[93] Skvortsov M A, Amini M and Kravtsov V E 2022 *Phys. Rev. B* **106** 054208
[94] Čadež T, Dietz B, Rosa D, Andreanov A, Slevin K and Ohtsuki T 2023 *Phys. Rev. B* **108** 184202
[95] Čadež T, Nandy D K, Rosa D, Andreanov A and Dietz B 2024 *New J. Phys.* **26** 083018
[96] Abrikosov A A 1957 *Sov. Phys. JETP* **5** 1174
[97] Zhang W, Zhang X, Che J and Dietz B 2024 *Eur. Phys. J. Spec. Top.* **233** 1275
[98] Dietz B 2022 *J. Phys. A: Math. Theor.* **55** 474003
[99] Legrand O, Mortessagne F and Weaver R L 1997 *Phys. Rev. E* **55** 7741
[100] Tudorovskiy T, Kuhl U and Stöckmann H J 2011 *J. Phys. A* **44** 135101
[101] Białous M, Yunko V, Bauch S, Ławniczak M, Dietz B and Sirko L 2016 *Phys. Rev. E* **94** 042211
[102] Šeba P 1990 *Phys. Rev. Lett.* **64** 1855
[103] Haake F, Lenz G, Šeba P, Stein J, Stöckmann H J and Życzkowski K 1991 Phys
[104] Šeba P and Życzkowski K 1991 *Phys. Rev. A* **44** 3457
[105] Shigehara T, Yoshinaga N, Cheon T and Mizusaki T 1993 *Phys. Rev. E* **47** R3822
[106] Weaver R L and Sornette D 1995 *Phys. Rev. E* **52** 3341
[107] Rahav S and Fishman S 2002 *Nonlinearity* **15** 1541
[108] Zhang R, Zhang W, Dietz B, Chai G and Huang L 2019 *Chin. Phys. B* **28** 100502
[109] Marks R 1991 *IEEE Trans. Microwave Theory Tech.* **39** 1205
[110] Rytting D K 2001 *Proc. ARFTG/NIST Short Course RF Measurements Wireless World* pp. 1–66
[111] Yeh J H and Anlage S M 2013 *Rev. Sc. Inst.* **84** 034706
[112] Dietz B, Klaus T, Masi M, Miski-Oglu M, Richter A, Skipa T and Wunderle M 2024 *Phys. Rev. E* **109** 034201
[113] Pandey A 1981 *Ann. Phys.* **134** 110
[114] Guhr T 1996 *Ann. Phys.* **250** 145
[115] Kota V K B and Sumedha S 1999 *Phys. Rev. E* **60** 3405
[116] Schierenberg S, Bruckmann F and Wettig T 2012 *Phys. Rev. E* **85** 061130
[117] Dietz B, Friedrich T, Harney H L, Miski-Oglu M, Richter A, Schäfer F and Weidenmüller H A 2007 *Phys. Rev. Lett.* **98** 074103
[118] Bohigas O and Giannoni M J 1974 *Ann. Phys.* **89** 393
[119] Oganesyan V and Huse D A 2007 *Phys. Rev. B* **75** 155111
[120] Atas Y Y, Bogomolny E, Giraud O and Roux G 2013 *Phys. Rev. Lett.* **110** 084101
[121] Atas Y, Bogomolny E, Giraud O, Vivo P and Vivo E 2013 *J. Phys. A* **46** 355204
[122] Bogomolny E and Giraud O 2002 *Nonlinearity* **15** 993
[123] Laurent D, Legrand O and Mortessagne F 2006 *Phys. Rev. E* **74** 046219
[124] Harish-Chandra M 1958 *Am. J. Math.* **80**